BIOCHEMISTRY
including biophysical chemistry & molecular biology

Article

pubs.acs.org/biochemistry

The C113D Mutation in Human Pin1 Causes Allosteric Structural Changes in the Phosphate Binding Pocket of the PPIase Domain through the Tug of War in the Dual-Histidine Motif

Ning Xu,[†] Naoya Tochio,[‡] Jing Wang,[†] Yu Tamari,[†] Jun-ichi Uewaki,[†,‡] Naoko Utsunomiya-Tate,[§] Kazuhiko Igarashi,[∥] Takuma Shiraki,[⊥] Naohiro Kobayashi,[@] and Shin-ichi Tate*[,†,‡]

[†]Department of Mathematical and Life Sciences, School of Science, Hiroshima University, 1-3-1 Kagamiyama, Higashi-Hiroshima 739-8526, Japan

[‡]Research Center for the Mathematics on Chromatin Live Dynamics (RcMcD), Hiroshima University, 1-3-1 Kagamiyama, Higashi-Hiroshima 739-8526, Japan

[§]Faculty of Pharma-Sciences, Teikyo University, 2-11-1, Kaga, Itabashik-ku, Tokyo 173-8605, Japan

[∥]Department of Biochemistry, Tohoku University Graduate School of Medicines, 2-1, Seiryo-machi, Aoba-ku, Sendai, Miyagi 980-0575, Japan

[⊥]Faculty of Biology-Oriented Science and Technology, Kinki University, 930 Nishimitani, Kinokawa, Wakayama 649-6493, Japan

[@]Institute for Protein Research, Osaka University, 3-2 Yamadaoka, Suita 565-0871, Japan

Supporting Information

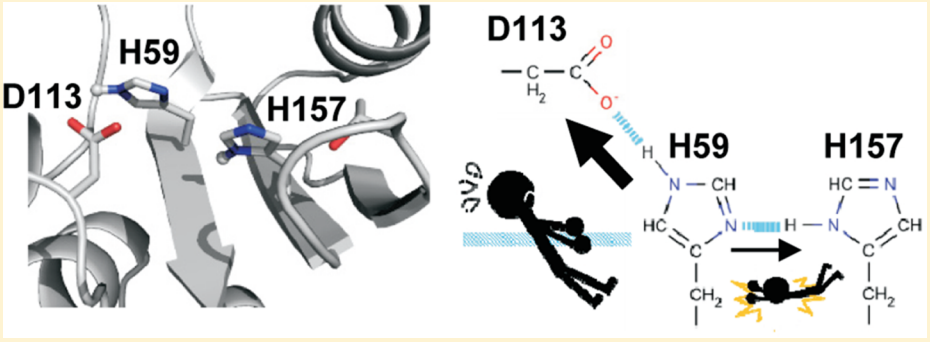

ABSTRACT: Pin1 peptidyl-prolyl isomerase (PPIase) catalyzes specifically the pSer/pThr-Pro motif. The *cis*−*trans* isomerization mechanism has been studied by various approaches, including X-ray crystallography, site-directed mutagenesis, and the kinetic isotope effect on isomerization. However, a complete picture of the reaction mechanism remains elusive. On the basis of the X-ray structure of Pin1, residue C113 was proposed to play a nucleophile attacker to catalyze the isomerization. The controversial result that the C113D Pin1 mutant retains the activity, albeit at a reduced level, challenges the importance of C113 as a catalyst. To facilitate our understanding of the Pin1 isomerization process, we compared the structures and dynamics of the wild type with those of the C113D mutant Pin1 PPIase domains (residues 51−163). We found the C113D mutation disturbed the hydrogen bonds between the conserved histidine residues, H59 and H157 ("dual-histidine motif"); H59 imidazole forms a stable hydrogen bond to H157 in the wild type, whereas it has a strong hydrogen bond to D113 with weakened bonding to H157 in the C113D mutant. The C113D mutation unbalanced the hydrogen bonding tug of war for H59 between C113/D113 and H157 and destabilized the catalytic site structure, which eventually resulted in an altered conformation of the basic triad (K63, R68, and R69) that binds to the phosphate group in a substrate. The change in the basic triad structure could explain the severely weakened substrate binding ability of the C113D mutant. Overall, this work demonstrated that C113 plays a role in keeping the catalytic site in an active fold, which has never before been described.

Pin1 is a highly conserved peptidyl-prolyl isomerase (PPIase) that specifically catalyzes the *cis*−*trans* isomerization of pSer/pThr-Pro substrates and thereby regulates protein functions.[1−3] Pin1 catalyzes the intrinsically slow conversion of the peptidyl-prolyl bond from *cis* to *trans* and vice versa, thus "switching" the pSer/pThr-Pro backbone conformation, and this switch is coupled with protein kinase activity toward the Ser/Thr-Pro motif. The Pin1-mediated conformational changes following phosphorylation are believed to constitute novel transduction pathways in various phosphor-

Received: June 24, 2014
Revised: August 2, 2014
Published: August 7, 2014

dx.doi.org/10.1021/bi5007817 | *Biochemistry* 2014, 53, 5568−5578

ylation-dependent signaling processes in cells. Dysfunctional Pin1, therefore, leads to the pathogenesis of cancer and protein folding diseases, including Parkinson's and Alzheimer's diseases.[4−6] Interactions of Pin1 with particular transcription factors that are phosphorylated in cells play essential roles in maintaining the pluripotency of induced pluripotent stem cells and embryonic stem cells.[7]

Pin1 is composed of two domains: a catalytic domain functioning as a PPIase and a WW domain that binds to pSer/pThr-Pro-containing substrates.[8] The two domains are shown to interplay when Pin1 acts,[9−11] whereas the PPIase domain is solely responsible for isomerization activity. Moreover, the isolated PPIase domain displays activity comparable to or greater than that of full-length Pin1;[12] thus, the use of the isolated PPIase domain for studying its enzyme mechanism is feasible.

Pin1 is a member of the parvulin family, which is a family of proteins that contain a small PPIases. Parvulins are classified into two types in terms of substrate specificity: phospho-specific (Pin1-type) and non-phospho-specific (Par14-type);[13] the non-phospho-specific type parvulins consist of only PPIase without a WW domain.[14] All parvulins share similar folds and conserved residues in the catalytic site of PPIase domains,[8] which allows a structural comparison among the parvulin PPIases for assessing the roles of each conserved catalytic site residue. The high-resolution crystal structure of human Par14 showed that the four conserved residues form a hydrogen bond network that runs across the catalytic site.[15] The hydrogen bond network by the four-residue motif ("catalytic tetrad") in Par14 is supposed to be conserved among all parvulin family PPIases to maintain the folding of the catalytic site.[15] The catalytic tetrad in Pin1 consists of C113, H59, H157, and T152, while the Par14 counterpart consists of D74, H42, H123, and T118. The tetrad motif sequence is, thus, represented as Cys/Asp-His-His-Thr/Ser with inclusion of the variation at the fourth residue in the parvulins.[15]

The Pin1 catalytic mechanism at the atomic level is not well understood. The proximity of C113 to the carbonyl in the bound Ala-Pro dipeptide in the Pin1 complex crystal structure deduced the nucleophile attack catalysis by C113.[8] The cysteine, however, does not seem to be essential, as evidenced by the observation that C113D and C113S mutations did not abolish activity.[16] Moreover, the corresponding cysteine is replaced with an aspartate in Par14-type PPIases.[14,17] In an alternative proposition, the SH group of C113 forms a hydrogen bond to a carbonyl oxygen of the substrate to disrupt the carbon−nitrogen π-bond of the amide to facilitate easy rotation of this bond.[16] This mechanism, however, cannot clearly explain the severe decrease in activity for the C113S mutation that replaces SH with OH, as both groups can work as hydrogen bond donors. An elaborate study using kinetic isotope effects demonstrated that twisting the amide bond decreases the transition energy for isomerization, which is facilitated by hydrogen bonding to a prolyl nitrogen from the following residue amide proton in the substrate peptide.[18] The crystal structure of Pin1 with a reduced amide inhibitor bound in the active site showed the compound structure was close to the twisted amide, which is proposed to exist in a transition state.[19]

Molecular dynamics simulations gave other insights into the *cis*−*trans* isomerization process. Hamelberg and co-workers applied molecular dynamics simulations to sample the entire conformational ensemble of the Pin1 substrate complex, with the corresponding relative binding free energies, during the *cis*−*trans* conversion of the substrate.[20] The theoretical work could assess the binding free energies in the substrate−Pin1 complex, which are not accessible experimentally, and showed that Pin1 preferentially binds to the transition state substrate with $\omega \approx 90°$ over those in the *cis* or *trans* state.[20] This observation is consistent with the twisted amide bond mechanism mentioned above.[18]

Hamelberg's group has also demonstrated that the PPIase domain of Pin1 in the free state samples conformations significantly wider than those for the complexes with a *cis* or *trans* peptide substrate.[21] They proposed that Pin1 adopts conformational selection in phosphorylated substrate recognition and emphasized the importance of the intrinsic structural flexibility of the Pin1 PPIase domain.[21] The functional relevance of the structural dynamics of PPIase domain is also emphasized experimentally: conformation sampling may change through contact with the WW domain in response to the substrate binding at the domain interface.[9−11]

In this work, we explored the mechanism to explain the reduced activity of the C113D Pin1 PPIase mutant with the intention of improving our understanding of how Pin1 isomerizes its substrate targets. The C113D mutant has raised controversial arguments against the currently proposed mechanisms. The crystal structure of Par14 proposed that the residues in the catalytic tetrad, defined as the Cys/Asp-His-His-Thr/Ser motif, are interconnected by hydrogen bonds and they play a role in properly positioning the Cys/Asp moiety to interact with a substrate.[15] However, this proposition appears to be invalid for Pin1, because the catalytic tetrad is kept in the C113D mutant as in the wild-type Pin1 PPIase domain, but the mutant shows significantly reduced activity. The maintenance of the catalytic tetrad structure per se does not explain the Pin1 PPIase function. In addition, the mechanism assuming the C113−substrate carbonyl interaction hardly explains why the C113D mutant retains activity, albeit reduced; the aspartate side chain cannot be a hydrogen bond donor at neutral pH, whereas the thiol group can be a hydrogen donor.[16] Exploring why the C113D Pin1 PPIase mutant has reduced activity should provide new insights into the isomerization mechanism of Pin1.

This work has shown that the reduced activity of C113D is primarily ascribed to its weakened binding to the phosphate moiety of the substrate. The reduced binding could be explained by the deformed active loop composed of three basic residues (K63, R68, and R69) that directly bind to the phosphate, as evidenced by the nuclear magnetic resonance (NMR) structures of both the C113D and wild-type Pin1 PPIases. The hydrogen bond between two histidines (H59 and H157) in the catalytic tetrad was observed in the wild-type Pin1 PPIase domain. The strength of the hydrogen bond, however, changed in the C113D mutant; H59 appears to be pulled to H157 in the wild type, whereas it has a stronger hydrogen bond to D113 in the C113D mutant. Thus, H59 is in a "tug of war" within the hydrogen bond network between the residue at position 113 and H157 in the catalytic tetrad. The imbalance of the tug of war by the C113D mutation altered the active loop structure, presumably by destabilizing the catalytic site fold. The structural destabilization by the C113D mutation was apparent, as evidenced by the elevated conformational exchanges seen in the spin relaxation data and the increased H/D exchange rates for most of the active site residues in the

dx.doi.org/10.1021/bi5007817 | *Biochemistry* 2014, 53, 5568−5578

C113D mutant. We emphasize that C113 plays a key role in maintaining the catalytic site in an active fold.

MATERIALS AND METHODS

Pin1 PPIase Purification. The cDNA encoding the peptidyl-prolyl isomerase (PPIase) domain of human Pin1 (residues 51−163)[8] was cloned into expression vector pET28a (Addgene Inc., Cambridge, MA). The recombinant plasmids were transformed into *Escherichia coli* strain BL21(DE3) cells (New England Biolabs Inc., Beverly, MA). The cells were grown in M9 minimal medium with 50 μg/mL kanamycin at 37 °C to an A_{600} of 0.6. For preparing the NMR samples, $^{15}NH_4Cl$ and [^{13}C]glucose were used as nitrogen and carbon sources, respectively. The expression of the His_6-tagged protein was induced by adding isopropyl β-thiogalactopyranoside to a final concentration of 0.5 mM, and cells were further cultured for 16 h at 18 °C. Cells from a 1 L culture medium were harvested and resuspended in 100 mL of a buffer solution [50 mM Tris-HCl (pH 8.0)]. The cells were disrupted by sonication, and the soluble fraction was collected by centrifugation at 26740*g* for 20 min at 4 °C. Polyethylenimine was added to the supernatant to a final concentration of 0.1% to remove the DNA and RNA contaminants by applying another centrifugation at 26740*g* for 20 min at 4 °C. The collected supernatant was applied to a TALON column (Takara Bio). After the flow through with buffer [50 mM Tris-HCl (pH 8.0)], the column was further washed with a 200 mL solution containing 50 mM Tris-HCl (pH 8.0) and 25 mM imidazole. The His_6-tagged protein was eluted with a different buffer solution [50 mM Tris-HCl (pH 8.0) and 400 mM imidazole]. The collected His_6-tagged protein was subjected to extensive dialysis against 50 mM sodium phosphate buffer (pH 6.0). After dialysis, 80 units of a thrombin protease solution (GE Healthcare) was added to the protein solution to cleave the His_6 tag from the PPIase domain fragment; the proteolysis reaction was performed at 20 °C overnight. The reactant was applied to a cation exchange HiTrap SP FF column (GE Healthcare) equilibrated with 50 mM sodium phosphate buffer (pH 6.0). The PPIase domain was eluted with a NaCl gradient from 0 to 1 M in 50 mM sodium phosphate buffer (pH 6.0) using a BioLogic DuoFlow HPLC system (Bio-Rad). The collected fractions containing PPIase were subjected to extensive dialysis against the desired buffer solutions according to the purposes of future use.

Site-directed mutagenesis to change C113 to D113 in the Pin1 PPIase domain was conducted by KOD FX (Toyobo, Osaka, Japan). The purification of C113D mutant PPIase was conducted according to the same protocol described above for the wild-type PPIase.

NMR Spectroscopy and Structure Determination. Structures of wild-type and C113D PPIases were determined according to the standard procedure using isotope-labeled samples.[22] A set of standard three-dimensional (3D) triple-resonance data was used to assign backbone and side chain resonances. NOEs from ^{15}N-edited and ^{13}C-edited 3D NOESY spectra were used to generate the distance restraints in the structure calculations. All NMR data were collected on a Bruker Avance II spectrometer equipped with a triple-resonance cryogenic probe operating at 700.33 MHz for the ^{1}H resonance frequency. Both wild-type and C113D mutant PPIases were dissolved in a buffer solution consisting of 50 mM sodium phosphate (pH 6.6), 100 mM Na_2SO_4, 5 mM ethylenediaminetetraacetic acid (EDTA), 1 mM DTT, and 0.03% NaN_3. All experiments were conducted at 299 K. NMR data were processed by NMRPipe,[23] and the spectral analyses were conducted using the program suite KUJIRA[24] running with NMRview.[25]

Structure calculations were conducted with CYANA 2.1 for fully automatic NOE assignments.[26,27] The backbone dihedral angle restraints were generated with TALOS+.[28] The 40 lowest-energy CYANA structures were subjected to explicit water refinement with XPLOR-NIH[29] with distance and dihedral restraints. The final 10 XPLOR-NIH structures were validated using PROCHECK-NMR.[30] The structural statistics for the wild-type and C113D mutant PPIases are provided as Supporting Information (Table S1).

The resonance assignments and the structural data for wild-type and C113D mutant PPIases have been deposited in the Biological Magnetic Resonances Bank (BMRB) and the Protein Data Bank (PDB): BMRB accession codes 11559 and 11560 and PDB entries 2RUC and 2RUD, respectively.

Isothermal Titration Calorimetry (ITC) Experiments. ITC experiments were conducted at two temperatures, 288 and 298 K, on a Microcal Auto-iTC200 calorimeter (GE Healthcare). The Cdc25C peptide (sequence of EQPLpTPVTDL, where pT represents a phosphorylated threonine) was dissolved in a 50 mM Tris-HCl buffer solution (pH 6.8). The peptide was titrated into a 200 μL PPIase solution [0.1 mM protein and 50 mM Tris-HCl (pH 6.8)]; 1.5 μL of a peptide solution (concentration of 1.2 mM) was injected at each of the 25 titrations. The collected data were analyzed using Microcal ORIGIN (GE Healthcare). The Cdc25C phosphorylated peptide was purchased from Funakoshi (Tokyo, Japan) and used without further purification.

Isomerization Rate Measurements. Isomerase activities for wild-type and C113D mutant PPIases were assessed by two-dimensional (2D) ^{1}H−^{1}H exchange spectroscopy (EXSY).[9,31] The sample contained 2 mM Cdc25C phosphopeptide with 50 μM PPIase (wild-type or C113D). The sample solution contained 50 mM Tris-HCl (pH 6.8), 1 mM DTT, and 0.03% NaN_3. The experiments were conducted at 295 K on a 700 MHz NMR spectrometer. The exchange times were set to 2, 5, 10, 15, 25, 35, 50 (twice), 75, 100 (twice), 200, 300, and 400 ms. The net exchange rate, k_{EX}, was estimated to fit the equation below (eq 1) to the ratios of the *trans*-to-*cis* exchange cross-peaks against the *trans* diagonal peaks. In estimating the k_{EX} values, we simultaneously used the buildup profiles from the signals for pT5 CH_3, pT5 HN, and V7 HN for fitting, as in a global fitting manner.

$$\text{ratio}(t_{mix}) = \frac{[1 - e^{-(k_{CT}+k_{TC})t_{mix}}]k_{TC}}{k_{CT} + k_{TC}e^{-(k_{CT}+k_{TC})t_{mix}}} \quad (1)$$

where k_{CT} and k_{TC} are adjustable parameters in fitting and the net exchange rate, k_{EX}, is defined as $k_{EX} = k_{CT} + k_{TC}$, where k_{CT} and k_{TC} are the exchange rates from *cis* to *trans* and *trans* to *cis*, respectively.[9] Uncertainties in the rate constants were estimated by Monte Carlo simulations on the basis of the duplicated data.

NMR Spin Relaxation Experiments and Analysis. All backbone ^{15}N R_1 and R_2 relaxation rates and steady state heteronuclear ^{15}N NOE (hNOE) data were collected on a 700 MHz NMR spectrometer at 299 K. Each peak intensity was measured by averaging over the signal intensities at the peak center and its eight surrounding points (nine-point averaging); each peak center was found by the SPARKY "pc" function (T. D. Goddard and D. G. Kneller, *SPARKY* 3, University of California, San Francisco). The delays for R_1 measurements

dx.doi.org/10.1021/bi5007817 | *Biochemistry* 2014, 53, 5568−5578

(t_{relax}) were 10.3 (twice), 153.9, 307.9, 461.8, 615.7 (twice), 769.6, 923.6, 1128.8, and 1539.3 ms, whereas the delays for R_2 (t_{relax}) were 0.0, 16.0 (twice), 40.0, 80.0 (twice), and 160.0 ms. The spectra for R_1 and R_2 were collected in an interleaved manner. For measuring hNOEs, we recorded an interleaved pair of spectra in which ^{1}H saturation of 3 s was applied alternatively with the relaxation delay set to 2 s.

R_1 and R_2 relaxation rate constants for each signal were determined through the function fitting using the modelXY TCL built-in function of NMRPipe. Uncertainties for R_1 and R_2 were estimated in a Monte Carlo manner on the basis of the duplicated data. The uncertainty for each hNOE value was evaluated using the root-mean-square deviation value on a spectral region with no peaks, which was obtained by the NMRPipe built-in module.

The reduced spectral density functions, including $J_{eff}(0)$, $J(\omega_H)$, and $J(\omega_N)$, were calculated using the software suite REALAX version 3.1.5.[32,33] Rotational correlation times and the rotation diffusion tensors for the wild type and C113D mutant were determined by RotDif[34] on the Matlab platform (Mathworks).

H/D Exchange Rate Measurements. The amide proton/deuteron exchange (H/D exchange) rates were measured with extensively lyophilized samples; the sample solution [wild-type or C113D mutant PPIase in 50 mM sodium phosphate (pH 6.6), 100 mM Na_2SO_4, 5 mM EDTA, 1 mM DTT, and 0.03% NaN_3] was rapidly frozen in liquid nitrogen and placed into a vacuum chamber for ~12 h. To remove the remaining protons from the sample, the lyophilized sample described above was again dissolved with 100 μL of D_2O [over 99.96 atom % deuterium (Sigma-Aldrich)] and again lyophilized. The lyophilized sample in a plastic test tube was dissolved with the same volume of D_2O as the volume that evaporated, just prior to the recording of a series of 2D ^{1}H−^{15}N HSQC spectra. The NMR measure was initiated within 10 min after dissolving the sample. For the case of the wild type, one spectrum was collected for 25 min and 24 data sets were collected sequentially. For the C113D mutant, it took 35 min for one spectrum and 35 spectra were measured sequentially. There was no apparent structural change caused by lyophilization to both wild-type and C113D PPIases, which was evidenced by an NMR spectral comparison between the data before and after lyophilization. H/D exchange rates for each peak were determined through the peak intensity change according to the measuring time; the time at the end of each spectral collection was used as the H/D exchange delay time for the signals on the corresponding spectrum. In functional fitting to extract the H/D exchange rate, $R_{H\rightarrow D}$, the incomplete exchange of ^{1}HN to ^{2}DN due to the residual proton content of the D_2O solution was considered; the function in eq 2 was, thus, used for fitting to the HN intensity profile

$$I(t) = I_0 \exp(-R_{H\rightarrow D}t) + I_b \quad (2)$$

where I_0, I_b, and $R_{H\rightarrow D}$ are used as the adjustable parameters in fitting calculations.

R_2 Relaxation Dispersion Experiments. Conformational exchange rates were further elucidated by using R_2 relaxation dispersion experiments using a series of ^{15}N CPMG-HSQC spectra.[35] The effective transverse relaxation rates were measured by changing the delays between 180° pulses for ^{15}N spins in the CPMG loop. The total CPMG duration was held constant at 40 ms. Samples contained 1.4 mM (wild-type) and 2.0 mM (C113D mutant) protein in 50 mM sodium phosphate (pH 6.6), 100 mM Na_2SO_4, 1 mM DTT, 0.03% NaN_3, and 5 mM EDTA. The samples in 50 mM Tris-HCl (pH 6.8), 1 mM DTT, and 0.03% NaN_3 contained 0.3 mM protein for both wild-type and C113D mutant PPIases. All the experiments were conducted at 299 K on a Bruker Avance II 700 MHz NMR spectrometer. Each peak intensity was estimated by nine-point averaging for each cross-peak using a home-written program.

Kinetic parameters were estimated by using a two-state model of the general Carver−Richards equation.[36] Functional fitting to the data was achieved by using a home-written program adopting the differential evolution optimization.[37] Uncertainties were estimated on the basis of duplicate data and a Monte Carlo approach, in which 32 data sets of each residue were generated on the basis of an initial fit of the collected data to which Gaussian noise representing experimental uncertainties of R_2 was added. Exchanging residues were grouped according to their individual R_2 rates, and the residues in each group were subjected to global fitting to gain a single R_2 value for all the residues in the same group. Uncertainties for the global kinetic parameter were estimated by a Monte Carlo approach.

Measuring Histidine Imidazole ^{15}N Chemical Shift Changes According to the D_2O Content in Solution. The imidazole ^{15}N chemical shifts were measured using 2D ^{1}H−^{15}N HSQC spectra for sample solutions containing 6, 50, and 100% D_2O. The sample was prepared from the lyophilized protein solution containing 50 mM sodium phosphate buffer (pH 6.6) and 100 mM sodium sulfate. To exclusively eliminate the proton, the lyophilized sample was dissolved by D_2O and then subjected to further lyophilization; the procedure was repeated twice to extensively purge protons from the sample. In the final sample solution containing different amounts of D_2O, 5 mM EDTA, 1 mM DTT, and 0.03% NaN_3 were added. All data were collected at 299 K on a 700 MHz NMR spectrometer.

RESULTS

***cis*−*trans* Isomerization Rates for Wild-Type and C113D Mutant PPIases.** C113D mutant Pin1 PPIase showed a significant reduction in k_{cat} relative to that of the wild type.[16] To further elucidate the role of C113 in the isomerization process, we directly measured the *cis*−*trans* isomerization rates for the wild-type and C113D mutant PPIase domains using 2D EXSY (Figure 1A). In what follows, we refer to the Pin1 PPIase domain as simply PPIase, unless otherwise noted. The Cdc25C phosphorylated peptide was used as the substrate. The *cis*−*trans* isomerization rates were 51.6 ± 1.9 s^{-1} (wild type) and 0.7 ± 0.5 s^{-1} (C113D mutant) at 295 K. The rates for *trans*−*cis* exchange were 6.6 ± 2.1 s^{-1} (wild type) and 0.1 ± 0.0 s^{-1} (C113D mutant). The isomerase activity of C113D was approximately 70-fold lower than that of the wild type.

C113D Mutant PPIase Showed Limited Affinity for the Phosphorylated Peptide. The binding affinity for the phosphorylated peptide was compared with ITC data (Figure 1B). The results demonstrated that the C113D mutant PPIase has very limited affinity for the phosphopeptide with apparently no binding observed, whereas the wild type showed a dissociation constant (K_D) of ≈10 mM. The reduced isomerization rate of the C113D mutant is ascribed to its faint substrate affinity.

Structural Change Induced by the C113D Mutation Assessed by NMR Chemical Shifts. Comparison of 2D ^{1}H−^{15}N HSQC spectra for the wild-type and C113D mutant

dx.doi.org/10.1021/bi5007817 | *Biochemistry* 2014, 53, 5568−5578

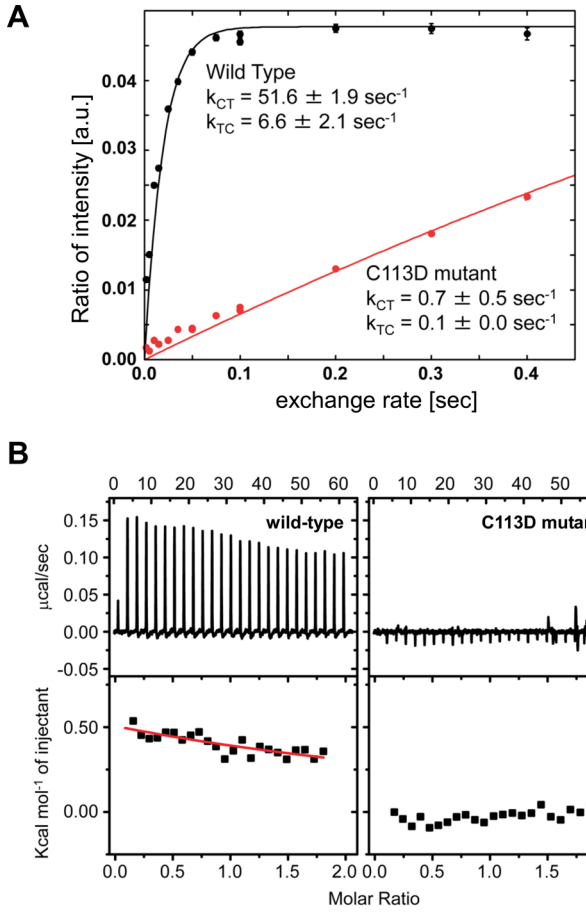

Figure 1. (A) Experimental rate constants for the wild type and C113D mutant were measured by EXSY with the Cdc25C phosphorylated peptide at varying exchange times. (B) Isothermal calorimetric titration data for the wild-type (left) and C113D mutant (right) PPIase domains at 298 K. Each peak corresponds to 1.5 μL injections of the Cdc25C phosphorylated peptide substrate solution. The solid red line drawn in the wild-type ΔH plot (bottom left) is the best-fit model function assuming a 1:1 protein:substrate stoichiometry.

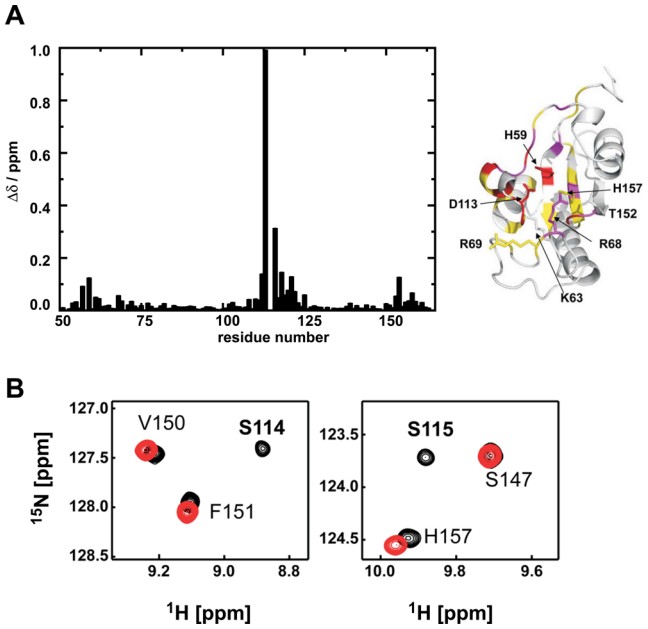

Figure 2. (A) Residue-wise plot for the normalized chemical shift differences between the wild type and the C113D mutant. The normalized chemical shift difference for each residue is defined as $\Delta\delta = [(\Delta\delta^{1}\mathrm{H})^2 + (\Delta\delta^{15}\mathrm{N}/5)^2]^{1/2}$, where $\Delta\delta^{1}$H and $\Delta\delta^{15}$N are the chemical shift differences in the ^{1}H and ^{15}N dimensions, respectively.[48] According to the magnitude of $\Delta\delta$, the residues in the C113D mutant structure were colored differently: red for $>\Delta\delta_{ave} + 1\sigma$, purple for $>\Delta\delta_{ave} + 0.5\sigma$, and yellow for $>\Delta\delta_{ave} + 0.25\sigma$, where $\Delta\delta_{ave}$ is the average value for $\Delta\delta$ and σ is the standard deviation of $\Delta\sigma$ calculated over all residues. (B) Overlaid presentation of parts of the 2D ^{1}H−^{15}N spectra for the wild type (black) and the C113D mutant (red), which shows that the signals for S114 (left) and S115 (right) have disappeared in the spectrum for the C113D mutant. The S114 signal was observed far from the displayed spectral region with very weak intensity, while the S115 resonance was not observed in the spectrum for the C113D mutant.

PPIases showed that the C113D mutation caused spectral changes to a wide range of residues in the catalytic site (Figure 2A). Residues K63, R68, and R69 showed significant spectral changes, implying the mutation may disturb the distal loop in an allosteric manner (Figure 2A, right).

S114 and S115, which neighbor the mutation site, showed a severe reduction in their signal intensities (Figure 2B). The signal for S114 in the C113D mutant was observed at 8.80 ppm (^{1}H) and 120.6 ppm (^{15}N) in the spectrum with extremely weak intensity, whereas the S115 signal was not observed. The C113D mutation could facilitate their amide proton exchange with water by proximate positioning of the negatively charged aspartate side chain to the amide groups of S114 and S115.[38]

Structural Changes Caused by the C113D Mutation. Three-dimensional structures for the wild type and C113D mutant were compared, which were determined by NMR under the same experimental conditions (Figure 3 and Figure S1 of the Supporting Information). The overlaid structures for the wild-type and C113D PPIase demonstrated that the apparent structural changes are in the helix near the mutation site and the active site loop (residues K63−T81) (Figure 3A). In the following section, the observed structural differences will be described in detail.

The structures near C113 showed subtle but significant changes. The short helix including S114 and S115 was extended in the mutant (Figure 3B). This extended helix could allow the amide groups of S114 and S115 to be close to the side chain negative charge of D113 for a time longer than that observed for the corresponding residues in the wild type, which may explain the reduced signal intensities for S114 and S115 in the C113D mutant (Figure 2B).

Taking a closer examination of the active site loop (residues K63−T81) in the C113D mutant showed that the backbone structure changed compared with the same region in the wild-type protein to reorient the side chains of residues K63, R68, and R69, which are termed the "basic triad" (Figure 3C). The crystal structure of a reduced amide−Pin1 complex (PDB entry 3NTP), where the structure is considered to mimic the transition state complex with pSer-Pro, showed that the basic triad residues form hydrogen bonds to the phosphate moiety in the substrate.[19] The side chain reorientation of the basic triad in the C113D mutant may explain the severely reduced capacity for binding to the phosphorylated substrate (Figure 1B).

To support the discussion presented above about the C113D active loop structure, it should be noted that the active loop maintains structural rigidity that is comparable to the secondary structure regions, as evidenced by the hNOE values of >0.8, in both the wild type and the C113D mutant (Figure S2 of the

dx.doi.org/10.1021/bi5007817 | Biochemistry 2014, 53, 5568−5578

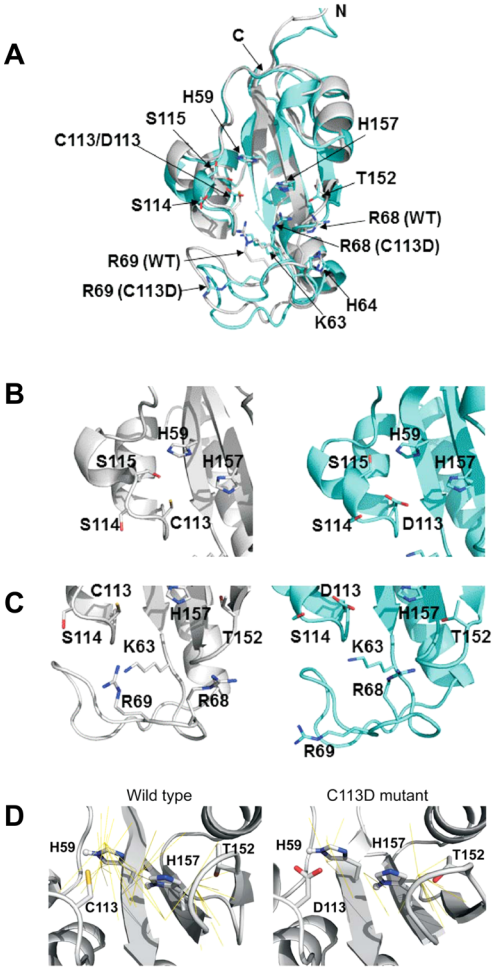

Figure 3. (A) Structural overlap between the wild-type (gray) and C113D mutant (blue) PPIase domains determined in this work. (B) Close-up view of the structures near the mutation site of the wild type (left, gray) and C113D mutant (right, blue). (C) Active loop structure composed of the basic triad of K63, R68, and R69 for the wild type (left, gray) and C113D mutant (right, blue). (D) Observed NOEs from the imidazole ring protons are drawn as yellow lines for the wild type (left) and C113D mutant (right). All figures were created with PyMOL (Schrödinger, LLC).

Supporting Information). The structural change observed for the loop is, therefore, significant (Figure 3C). In general, the accuracy and precision for a segment in an NMR structure tend to be poorly resolved, if the segment has apparent structural flexibility indicated by low hNOE values (typically, <0.5); however, this is not the case for this loop.

The structural determinations of the wild-type and C113D mutant PPIases were conducted in a solution containing 50 mM sodium phosphate and 100 mM Na_2SO_4. In the sample solution, phosphate or sulfate ions should stay in the phosphate binding pocket formed by the basic triad in both the wild type and C113D mutant; this was evidenced by the chemical shift changes between the spectra for the proteins in solution with and without phosphate and sulfate ions (Figure S3 of the Supporting Information). The basic triad structures in the wild type and C113D mutant (Figure 3C) could serve as surrogates for the phosphor moiety-bound state, which may consolidate the functional significance of the structural changes in the basic triad.

The C113D mutation destabilized the neighboring histidine cluster comprising H59 and H157. This is supported by the number of NOEs from the histidine ring protons being significantly smaller for the C113D mutant than for the wild type (Figure 3D); if fluctuations for interproton distances are significant, the observed NOE intensities for coupled systems should be reduced.[39]

Although the spatial arrangement of the imidazole rings of H59 and H157 in C113D is close to that in the wild type, their side chain dynamics should increase in the mutant.

Histidine Hydrogen Bond Stabilities Elucidated Using H/D Isotope Effects on NMR Chemical Shifts. In accordance with the destabilization of the histidine cluster in the catalytic site, the C113D mutation perturbed the hydrogen bonds mediated by H59 and H157. This was probed by the H/D isotope effect on the ^{15}N chemical shifts for their ring moieties. The direct attachment of the deuteron to the ^{15}N atom changes the ^{15}N chemical shifts according to the "hydron" (referring to proton or deuteron) position in the hydrogen bond; the secondary isotope effect is defined as $\Delta\delta(DN) = \delta(DN) - \delta(HN)$, where $\delta(DN)$ and $\delta(HN)$ denote the ^{15}N chemical shift values when the structure is bonded to a deuteron and a proton, respectively.[40]

The tautomeric forms for H59 and H157 in Pin1 PPIase were determined by 2D $^1H-^{15}N$ HSQC spectra using the $^1H^{\varepsilon 1}$ and $^1H^{\delta 2}$ nuclei in the imidazole rings;[41] H59 $N^{\varepsilon 2}$ and H157 $N^{\delta 1}$ are directly bound to a proton (Figure S4 of the Supporting Information). The ^{15}N chemical shifts for $N^{\varepsilon 2}$ (H59) and $N^{\delta 1}$ (H157) showed high-field isotope shifts when the structure was bound to a deuteron, suggesting that these nitrogen atoms are hydrogen bond donors (Figure 4).[40] The identified tautomeric forms for the histidine imidazole rings were used in the structure calculation to define their ring orientation (Figure 3D). The imidazole ring flips for H59 and H157 were the same between the wild-type and C113D mutant Pin1 PPIase; their ring orientations were similar to those found in the high-resolution Par14 crystal structure.[15] As expected from the Par14 structure, the hydrogen bonds between $H^{\varepsilon 2}$ (H59) and $H^{\delta 1}$ (H157) can form hydrogen bonds to the C113 (D113) side chain S^{γ} (O^{δ}) atom and the H59 $N^{\delta 1}$ atom, respectively.

The stability of each hydrogen bond was elucidated on the basis of the rates of chemical exchange between the ND and NH states in a solution containing 50% D_2O (Figure 4). As demonstrated in parts of the spectra, the signal line shapes for $N^{\varepsilon 2}$ (H59) and $N^{\delta 1}$ (H157) observed in a 50% D_2O solution were different between the wild type and the C113D mutant, implying the hydrogen bonds in the histidine cluster changed in the C113D mutant active site (Figure 4). $N^{\delta 1}$ (H157) in the wild-type PPIase was a doublet along the ^{15}N axis, while the counterpart signal in the C113D mutant was a singlet resonating at the midpoint of the chemical shifts between $\delta(N^{\delta 1}H)$ and $\delta(N^{\delta 1}D)$ (Figure 4A). In the case of $N^{\varepsilon 2}$ (H59), the wild type showed a singlet but the corresponding signal from the C113D mutant showed a doublet (Figure 4B). The doublet signals in a 50% D_2O solution indicate slow H/D exchange onto the corresponding ^{15}N nucleus. On the basis of the isotope shift of $\delta(^{15}N)$ of approximately −1.0 ppm (Figure 4), the H/D exchange rate for the proton on the ^{15}N nucleus was estimated to be <155 s^{-1}. The ^{15}N imidazole nitrogen atoms showing a doublet should be engaged in a stable hydrogen bond.

The imidazole ring orientations determined in the wild type and C113D mutant aided identification of the hydrogen bond

dx.doi.org/10.1021/bi5007817 | *Biochemistry* 2014, 53, 5568−5578

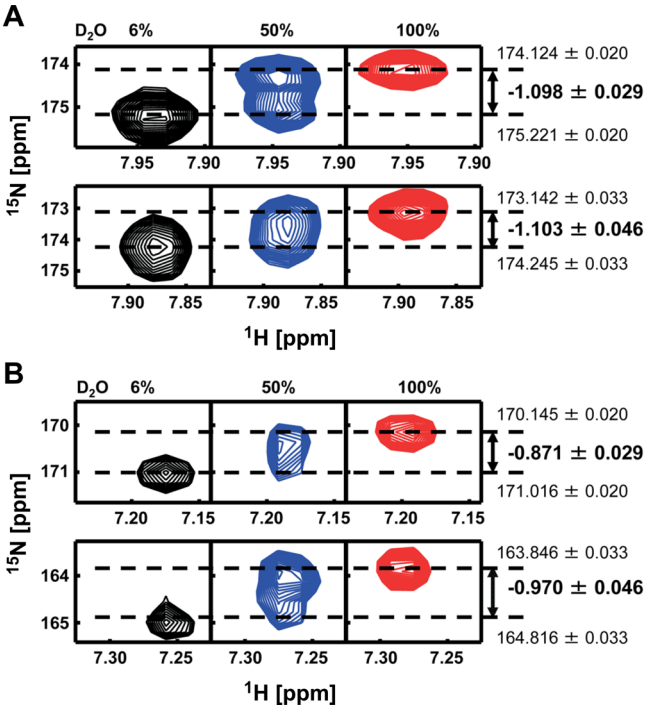

Figure 4. H/D isotope effects on the chemical shifts for ^{15}N nuclei in the histidine imidazole ring were measured in solutions with different D_2O contents. (A) 2D $^{1}H-^{15}N^{\delta 1}$ HSQC signals for H157 collected in the solution containing 6% (black, left), 50% (blue, middle), and 100% D_2O (red, right). Data in the top and bottom panels are for the wild type and C113D mutant, respectively. (B) Same data set for 2D $^{1}H-^{15}N^{\varepsilon 2}$ signals for H59 of the wild type (top) and C113D mutant (bottom).

network connecting residues C113/D113, H59, H157, and T152 and are formed across the active site irrespective of the mutation, as found in the Par14 crystal structure.[15] In assuming the hydrogen bond network, the $^{15}N^{\varepsilon 2}$ (H59) doublet in the C113D mutant may indicate that a stable hydrogen bond is formed between D113 O^{δ} and H59 $H^{\varepsilon 2}$ in C113D, whereas the $^{15}N^{\delta 1}$ (H157) doublet indicates a stable hydrogen bond is formed by $H^{\delta 1}$ (H157) and $N^{\delta 1}$ of H59 in the wild-type protein with a reduction in the stability of the hydrogen bond between $H^{\varepsilon 2}$ (H59) and the C113 side chain sulfur, S^{γ}.

The C113D Mutation Reduced Structural Stability As Determined by Enhanced Amide H/D Exchange. The residue-specific amide H/D exchange rates were measured from sequentially collected 2D $^{1}H-^{15}N$ HSQC spectra for both the wild type and C113D mutant. The exchange rates were determined for all residues observed in the first 2D $^{1}H-^{15}N$ HSQC spectrum just after mixing D_2O with the lyophilized sample. Most of the residues in the C113D mutant showed H/D exchange rates enhanced relative to those of the residues of the wild-type protein (Figure 5), implying the structure of the C113D mutant PPIase is less stable than that of the wild type.

Comparison of the Reduced Spectral Density Maps between the Wild Type and C113D Mutant. To characterize the changes in structural dynamics caused by the C113D mutation, we compared the reduced spectral density function results between the wild type and the C113D mutant.[42]

The difference [i.e., $\Delta J_{eff}(0) = J_{eff}(0)[C113D] - J_{eff}(0)[wild\text{-}type]$] in the $J_{eff}(0)$ values between the wild type and C113D mutant were plotted against the residue number (Figure 6).

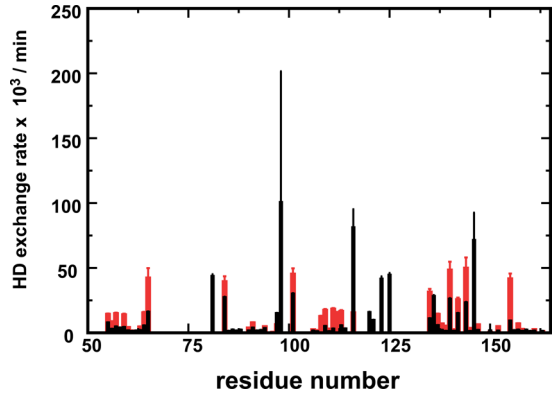

Figure 5. H/D exchange rates for residues in the wild type (black) and the C113D mutant (red). The residues without exchange rates showed no observable peaks in the first 2D $^{1}H-^{15}N$ HSQC spectrum recorded in the data series collected, implying their amide protons have rapidly exchanged to deuterons within ≈10 min.

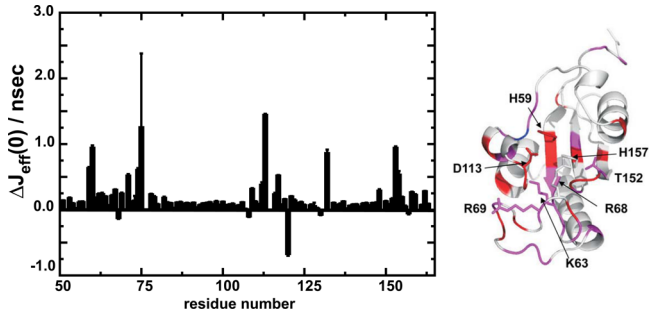

Figure 6. Plot for the residue-wise difference in spectral density function $J_{eff}(0)$. The difference was calculated for each residue as $\Delta J_{eff}(0) = J_{eff}(0)^{C113D} - J_{eff}(0)^{wild\text{-}type}$, where $J_{eff}(0)^{C113D}$ and $J_{eff}(0)^{wild\text{-}type}$ are the values for the C113D mutant and the wild-type protein, respectively. The residues in the C113D mutant structure are colored according to the magnitude of the $\Delta J_{eff}(0)$ value: red for $>\Delta J_{eff}(0)_{ave} + 1\sigma$, magenta for $>\Delta J_{eff}(0)_{ave} + 0.5\sigma$, blue for $<\Delta J_{eff}(0)_{ave} - 1\sigma$, and cyan for $<\Delta J_{eff}(0)_{ave} - 0.5\sigma$.

Most of the residues in C113D showed $J_{eff}(0)$ values larger than those for the corresponding residues in the wild type (Figure 6). $J_{eff}(0)$ depends on the R_2 rate, and if chemical exchange is present, the corresponding $J_{eff}(0)$ value increases accordingly.[26]

The hNOE profiles for the wild-type and C113D mutant PPIase are close to each other (Figure S2 of the Supporting Information), implying that the C113D mutation does not apparently affect the structural dynamics in the nanosecond to picosecond time range. The rotational correlation time, τ_c, was estimated for the wild type and C113D mutant. When the rotational diffusion anisotropy was taken into consideration,[34] the τ_c values for the wild type and C113D mutant were 9.4 ± 0.4 and 9.5 ± 0.5 ns, respectively, with rotational diffusion tensor anisotropy values of 1.3 ± 0.1 and 1.2 ± 0.1, respectively. In both cases, the axially symmetric rotational diffusion tensor model was adopted with statistical significance. As estimated above, the correlation time does not change when the C113D mutation in introduced. The minimal differences in the dynamic parameters for the motion on the picosecond to nanosecond time scale between the two constructs does not explain the observed differences in $J_{eff}(0)$. The increased $J_{eff}(0)$ values for residues in the C113D mutant, therefore, can be traced to an increase in chemical exchange terms for the R_2 rates. This observation implies that the majority of the C113D

dx.doi.org/10.1021/bi5007817 | Biochemistry 2014, 53, 5568−5578

mutant becomes structurally unstable, leading to significant conformational exchange that is apparent in the microsecond to millisecond time regime.

The changes in the $J_{eff}(0)$ values are particularly apparent for residues in the phosphate binding pocket, especially residues 60−75 (Figure 6, right), suggesting the binding pocket becomes structurally unstable in the C113D mutant. This allosteric destabilization effect caused by the C113D mutation appears to be rather independent of the presence of the phosphate group in the binding pocket, as the residues in the active loop showed increased $J_{eff}(0)$ values in the mutant for the sample with no phosphate and sulfate ions present (Figure S5 of the Supporting Information). The higher-frequency reduced spectral density functions, $J(\omega_H)$ and $J(\omega_N)$, did not show any large differences between the wild-type and mutant proteins, although the absence of ions did lead to larger changes (Figures S6 and S7 of the Supporting Information). The entire profiles for the reduced spectral densities are compared in the Supporting Information (Figures S8 and S9).

R_2 relaxation dispersion experiments were used to further characterize the structural dynamics in the microsecond to millisecond time regime. However, the results were less informative because of the limited number of residues showing detectable R_2 dispersion profiles, as described in the preceding work (Table S2 of the Supporting Information).[43] It is noted that the changes in the structural dynamics revealed by the R_2 dispersion profiles were dependent on the coexistence of the phosphate and sulfate ions (Table S2 of the Supporting Information). The number of residues showing significant R_2 dispersion was larger for both the wild type and the C113D mutant when no ions were present in the buffer.

DISCUSSION

The C113D Mutation Destabilized the Active Fold of the Catalytic Site. The functional importance of C113 has been the focus since the first Pin1 crystal structure was reported.[8] This original proposition emphasizing the role the SH group plays as a catalyst in the *cis*−*trans* isomerization is, however, now called into question, because of several controversial results, including the fact that the C113D mutant does not abolish the isomerization activity even if it shows reduced enzyme ability.[16] Roles other than that of a catalyst are anticipated for C113.

In a line of the C113 characterization, this work demonstrated that C113 is important for keeping the proper fold of the catalytic site of the Pin1 PPIase domain. The C113D mutation destabilized the catalytic site structure, which was evidenced by the elevated H/D exchange rates (Figure 5), the facilitation of the ^{15}N spin transverse relaxation rates by the increased backbone conformational exchange (Figure 6), and the reduced folding stability measured by CD (Figure S10 of the Supporting Information). By impairing the catalytic site fold, the C113D mutation caused the allosteric structural change in the basic triad in the active loop of the PPIase domain (Figure 3C). The basic triad, comprising residues K63, R68, and R69, binds to the phosphate in a phosphorylated substrate.[8,19,20] The structural change in the basic triad could explain that the C113D mutant severely weakened its binding to the Cdc25C phosphorylated peptide by 70-fold (Figure 1A). The reduced isomerization activity of the C113D mutant is not caused by the lack of an SH group as a catalyst but by the allosteric structural change in the basic triad that weakens its binding to the phosphate in a substrate.

It is noted that the C113D mutation does not destroy the overall structure of the Pin1 PPIase domain, although its stability is reduced (Figure 3A and Figure S1 of the Supporting Information). We intuitionally think that the C113D mutation expands the backbone conformational states for the residues in the catalytic site, while keeping their average structure close to that of the wild type, which may explain the enhanced conformational exchange for the catalytic site residues (Figure 6).

The molecular dynamics simulation demonstrated that the Pin1 PPIase domain in a substrate free state adopts conformations wider than those allowed for the substrate-bound forms.[21] In considering the theoretical results, we prefer to think the C113D mutant could adopt conformational states wider than those for the wild type, because of the reduced folding stability of the mutant catalytic site.

The Folding Destabilization by the C113D Mutation Is Mediated by the Tug of War for H59. It is not readily understood why C113 plays a role in keeping the proper fold of the catalytic site from the structural comparison between the wild-type and C113D mutant PPIases (Figure 3A). Because the C113D mutation affected the dynamics of the residues widely spread over the catalytic site, the role of C113 should be realized through its interaction with the other residues (Figures 5 and 6).

In the NMR structures for the wild-type and C113D mutant PPIase domain, the imidazole ring flips for H59 and H157 and the spatial arrangements of the side chains of C113/D113 and T152 resemble the structures of the corresponding residues that form the hydrogen bond network among the catalytic tetrad in Par14 (Figure 3D).[15] It is feasible to think that the catalytic tetrad (residues C113, H59, H157, and T152) in Pin PPIase forms the same hydrogen bond network that is found in Par14.[15]

In the middle of the catalytic tetrad, there are two conserved histidines, H59 and H157, which is termed the "dual-histidine motif". This dual-histidine motif is shown to play a role in maintaining the Pin1 fold; the H59L mutation severely reduced the protein stability, while the H59L/H157L double mutation slightly restored the folding stability from that of the very unstable H59L.[44]

In this work, we showed that the C113D mutation altered the hydrogen bond between H59 and H157 by using H/D isotope effects on the imidazole ring ^{15}N chemical shifts (Figure 4). In the C113D mutant, the H59 ring has a stronger hydrogen bond presumably to the D113 side chain oxygen, whereas H59 has a stronger hydrogen bond to the H157 imidazole ring in the wild type (Figure 4). The change in the hydrogen bonds in the dual-histidine motif is reminiscent of a tug of war for H59 between C113/D113 and H157 (Figure 7A,B). In considering the essential role of H59 and the cooperative effect of H59 and H157 in the structural stability of Pin1, the weakened hydrogen bond between H59 and H157 rings in the C113D mutant could be related to the elevated structural dynamics of the C113D mutant (Figures 5 and 6).

The sulfur atom in the SH group is a poor hydrogen bond acceptor.[45] The change from an SH to OH group, therefore, can strengthen the hydrogen bond between D113 and H59 $N^{\varepsilon 2}$ in the C113D mutant, while concomitantly weakening the hydrogen bond to the H157 imidazole ring (Figure 7A,B). The reduced stability of the hydrogen bond between H59 and H157 could be confirmed by the reduced number of NOEs from the rings in two histidines in C113D relative to the number in the

dx.doi.org/10.1021/bi5007817 | *Biochemistry* 2014, 53, 5568−5578

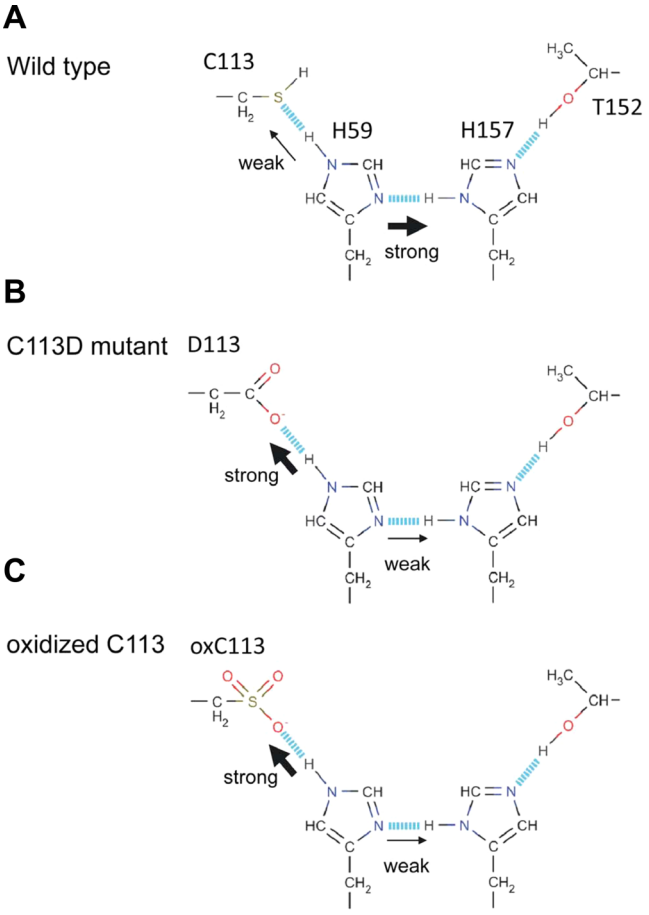

Figure 7. Hydrogen bond network and the tug of war for H59. (A) In the wild-type PPIase domain, H59 forms a stronger hydrogen bond to H157 than to C113. (B) In the C113D mutant, H59 strengthens the hydrogen bond to C113 while weakening the hydrogen bond to H157. (C) Oxidation of Pin1 PPIase preferentially converts the C113 thiol group to a sulfonate moiety, which resembles the D113 side chain structure. The oxygen atom in the sulfonate group functions as a better hydrogen bond acceptor than the sulfur atom of the thiol of C113. The oxidized C113 would strengthen the hydrogen bond from H59 while weakening the hydrogen bond between H59 and H157, as in the C113D mutant. The oxidized Pin1 is likely inactivated to a level that is comparable to that observed for the C113D Pin1 mutant.

wild type (Figure 3D). The sulfur atom in C113, therefore, should have a role in maintaining the well-balanced tug of war for H59 in the hydrogen bond network in the catalytic tetrad; the harder pulling of H59 to D113 unbalances the hydrogen bond network and, thus, results in the reduced stability of the catalytic site fold.

We should mention the biological significance in working on the C113D mutant. D113 is supposed to mimic the oxidized form of C113; the excessive oxidation to a SH group produces a sulfonic acid group (Figure 7C). C113 stays at the entrance of the catalytic cavity with the SH group exposed to solvent (Figure 3A), while the other cysteine, C57, in the Pin1 PPIase domain is buried in the structure. As anticipated from the structure, H_2O_2 specifically oxidized C113 while keeping C57 in its reduced form, which was assessed by using maleimide fluorescence labeling and mass spectroscopy (Figure S11 of the Supporting Information).

As reported, Alzheimer's disease (AD) brain is under oxidative stress that may be related to the pathogenesis and progression of AD.[46] Pin1 was found to be oxidized in AD hippocampus.[46] The oxidative modification of Pin1 resulted in reduced activity in the AD hippocampus, to an extent comparable to that seen in purified Pin1 treated with Fe^{2+} and H_2O_2.[46] From the work presented here, the oxidative modification to C113 in Pin1 can explain the significant reduction in the isomerization activity due to the binding of the impaired PPIase domain to the phosphate group in a phosphorylated substrate, without thinking of the excessive modifications like carbonyl adducts that are used as oxidative stress biomarkers.[47] The oxidation-prone C113 residue in Pin1 may link the reduced Pin1 activity and accumulation of phosphorylated tau protein in AD brain under oxidative stress, which leads to tangle formation and progression of AD.[3,46]

■ CONCLUSIONS

This study has demonstrated a novel role for C113 in stabilizing the catalytic site fold. The change from an SH to OH group disturbs the hydrogen bond network formed by the catalytic tetrad by unbalancing the tug of war for H59 between residues C113 and H157 (Figure 7). The dual-histidine motif comprising the conserved H59 and H157 is important for maintaining the catalytic site in an active fold. The imbalance of the tag of war in the C113D mutant weakens the hydrogen bond within the dual-histidine motif, thus destabilizing the catalytic site fold. The disturbed hydrogen bond network in the catalytic tetrad leads to the allosteric disorder of the active loop, including the basic triad that binds to a phosphate moiety of the substrate. This disorder explains the weakened substrate binding ability of the C113D mutant. Pin1 oxidation in cells should reduce its isomerization activity by reducing the binding affinity toward the substrate, as postulated from the work on the C113D mutant being a surrogate for the oxidized form of the Pin1 PPIase domain.

■ ASSOCIATED CONTENT

Supporting Information

Supporting data (Figures S1−S11). This material is available free of charge via the Internet at http://pubs.acs.org.

■ AUTHOR INFORMATION

Corresponding Author

*Department of Mathematical and Life Sciences, School of Science, Hiroshima University, 1-3-1 Kagamiyama, Higashi-Hiroshima 739-8526, Japan. Telephone: +81-82-424-7387. E-mail: tate@hiroshima-u.ac.jp.

Funding

This work was supported by the Platform for Dynamic Approaches to Living System from the Ministry of Education, Culture, Sports, Science and Technology, Japan. S.-i.T. acknowledges the support from a Grant-in-Aid for Scientific Research (B) (Grant 26291015) and a Grant-in-Aid for Exploratory Research (Grant 26650023).

Notes

The authors declare no competing financial interest.

■ ACKNOWLEDGMENTS

We thank the Natural Science Center for Basic Research and Development (N-BARD) at Hiroshima University for the technical assistance in measuring mass spectra used for the characterization of the purified protein. We thank Mr. Taichi Sugawara (Tohoku University) for technical assistance.

■ ABBREVIATIONS

PEG, poly(ethylene glycol); DTT, dithiothreitol; PDB, Protein Data Bank; BMRB, Biological Magnetic Resonance Bank; NOE, nuclear Overhauser effect; NOESY, NOE spectroscopy; HSQC, heteronuclear single-quantum coherence; CPMG, Carr−Purcell−Meiboom−Gill; EXSY, exchange spectroscopy.

■ REFERENCES

(1) Lu, K. P. (2004) Pinning down cell signaling, cancer and Alzheimer's disease. *Trends Biochem. Sci. 29*, 200−209.

(2) Esnault, S., Shen, Z.-J., and Malter, J. S. (2008) Pinning Down Signaling in the Immune System: The Role of the Peptidyl-Prolyl Isomerase Pin1 in Immune Cell Function. *Crit. Rev. Immunol. 28*, 45−60.

(3) Butterfield, D. A., Abdul, H. M., Opii, W., Newman, S. F., Joshi, G., Ansari, M. A., and Sultana, R. (2006) Pin1 in Alzheimer's disease. *J. Neurochem. 98*, 1697−1706.

(4) Lim, J., and Lu, K. P. (2005) Pinning down phosphorylated tau and tauopathies. *Biochim. Biophys. Acta 1739*, 311−322.

(5) Balastik, M., Lim, J., Pastorino, L., and Lu, K. P. (2007) Pin1 in Alzheimer's disease: Multiple substrates, one regulatory mechanism? *Biochim. Biophys. Acta 1772*, 422−429.

(6) Theuerkorn, M., Fischer, G., and Schiene-Fischer, C. (2011) Prolyl cis/trans isomerase signalling pathways in cancer. *Curr. Opin. Pharmacol. 11*, 281−287.

(7) Cai, N., Li, M., Qu, J., Liu, G.-H., and Izpisua Belmonte, J. C. (2012) Post-translational modulation of pluripotency. *J. Mol. Cell Biol. 4*, 262−265.

(8) Ranganathan, R., Lu, K. P., Hunter, T., and Noel, J. P. (1997) Structural and Functional Analysis of the Mitotic Rotamase Pin1 Suggests Substrate Recognition Is Phosphorylation Dependent. *Cell 89*, 875−886.

(9) Wilson, K. A., Bouchard, J. J., and Peng, J. W. (2013) Interdomain Interactions Support Interdomain Communication in Human Pin1. *Biochemistry 52*, 6968−6981.

(10) Namanja, A. T., Wang, X. J., Xu, B., Mercedes-Camacho, A. Y., Wilson, K. A., Etzkorn, F. A., and Peng, J. W. (2011) Stereospecific gating of functional motions in Pin1. *Proc. Natl. Acad. Sci. U.S.A. 108*, 12289−12294.

(11) Matena, A., Sinnen, C., van den Boom, J., Wilms, C., Dybowski, J. N., Maltaner, R., Mueller, J. W., Link, N. M., Hoffmann, D., and Bayer, P. (2013) Transient Domain Interactions Enhance the Affinity of the Mitotic Regulator Pin1 toward Phosphorylated Peptide Ligands. *Structure 21*, 1769−1777.

(12) Peng, J. W., Wilson, B. D., and Namanja, A. T. (2009) Mapping the dynamics of ligand reorganization via $^{13}CH_3$ and $^{13}CH_2$ relaxation dispersion at natural abundance. *J. Biomol. NMR 45*, 171−183.

(13) Fanghanel, J., and Fischer, G. (2004) Insights into the catalytic mechanism of peptidyl prolyl cis/trans isomerases. *Front. Biosci. 9*, 3453−3478.

(14) Mueller, J. W., and Bayer, P. (2008) Small Family with Key Contacts: Par14 and Par17 Parvulin Proteins, Relatives of Pin1, Now Emerge in Biomedical Research. *Perspect. Med. Chem. 2*, 11−20.

(15) Mueller, J. W., Link, N. M., Matena, A., Hoppstock, L., Ruppel, A., Bayer, P., and Blankenfeldt, W. (2011) Crystallographic proof for an extended hydrogen-bonding network in small prolyl isomerases. *J. Am. Chem. Soc. 133*, 20096−20099.

(16) Behrsin, C. D., Bailey, M. L., Bateman, K. S., Hamilton, K. S., Wahl, L. M., Brandl, C. J., Shilton, B. H., and Litchfield, D. W. (2007) Functionally important residues in the peptidyl-prolyl isomerase Pin1 revealed by unigenic evolution. *J. Mol. Biol. 365*, 1143−1162.

(17) Sekerina, E., Rahfeld, J., Muller, J., Fanghanel, J., Rascher, C., Fischer, G., and Bayer, P. (2000) NMR solution structure of hPar14 reveals similarity to the peptidyl prolyl cis/trans isomerase domain of the mitotic regulator hPin1 but indicates a different functionality of the protein. *J. Mol. Biol. 301*, 1003−1017.

(18) Mercedes-Camacho, A. Y., Mullins, A. B., Mason, M. D., Xu, G. G., Mahoney, B. J., Wang, X., Peng, J. W., and Etzkorn, F. A. (2013) Kinetic Isotope Effects Support the Twisted Amide Mechanism of Pin1 Peptidyl-Prolyl Isomerase. *Biochemistry 52*, 7707−7713.

(19) Xu, G. G., Zhang, Y., Mercedes-Camacho, A. Y., and Etzkorn, F. A. (2011) A reduced-amide inhibitor of Pin1 binds in a conformation resembling a twisted-amide transition state. *Biochemistry 50*, 9545−9550.

(20) Velazquez, H. A., and Hamelberg, D. (2013) Conformation-Directed Catalysis and Coupled Enzyme−Substrate Dynamics in Pin1 Phosphorylation-Dependent Cis−Trans Isomerase. *J. Phys. Chem. B 117*, 11509−11517.

(21) Velazquez, H. A., and Hamelberg, D. (2011) Conformational Selection in the Recognition of Phosphorylated Substrates by the Catalytic Domain of Human Pin1. *Biochemistry 50*, 9605−9615.

(22) Cavanagh, J., Fairbrother, W. J., Palmer, A. G., III, and Skelton, N. J. (1996) *Heteronuclear NMR Experiments*, Academic Press, Inc., New York.

(23) Delaglio, F., Grzesiek, S., Vuister, G. W., Zhu, G., Pfeifer, J., and Bax, A. (1995) NMRPipe: A multidimensional spectral processing system based on UNIX pipes. *J. Biomol. NMR 6*, 277−293.

(24) Kobayashi, N., Iwahara, J., Koshiba, S., Tomizawa, T., Tochio, N., Güntert, P., Kigawa, T., and Yokoyama, S. (2007) KUJIRA, a package of integrated modules for systematic and interactive analysis of NMR data directed to high-throughput NMR structure studies. *J. Biomol. NMR 39*, 31−52.

(25) Johnson, B. (2004) Using NMRView to Visualize and Analyze the NMR Spectra of Macromolecules. In *Protein NMR Techniques* (Downing, A. K., Ed.) pp 313−352, Humana Press, Totowa, NJ.

(26) Güntert, P. (2004) Automated NMR Structure Calculation with CYANA. In *Protein NMR Techniques* (Downing, A. K., Ed.) pp 353−378, Humana Press, Totowa, NJ.

(27) Güntert, P. (2009) Automated structure determination from NMR spectra. *Eur. Biophys. J. 38*, 129−143.

(28) Shen, Y., Delaglio, F., Cornilescu, G., and Bax, A. (2009) TALOS+: A hybrid method for predicting protein backbone torsion angles from NMR chemical shifts. *J. Biomol. NMR 44*, 213−223.

(29) Schwieters, C. D., Kuszewski, J. J., Tjandra, N., and Marius Clore, G. (2003) The Xplor-NIH NMR molecular structure determination package. *J. Magn. Reson. 160*, 65−73.

(30) Laskowski, R., Rullmann, J., MacArthur, M., Kaptein, R., and Thornton, J. (1996) AQUA and PROCHECK-NMR: Programs for checking the quality of protein structures solved by NMR. *J. Biomol. NMR 8*, 477−486.

(31) Jeener, J., Meier, B. H., Bachmann, P., and Ernst, R. R. (1979) Investigation of exchange processes by two-dimensional NMR spectroscopy. *J. Chem. Phys. 71*, 4546−4553.

(32) d'Auvergne, E., and Gooley, P. (2008) Optimisation of NMR dynamic models I. Minimisation algorithms and their performance within the model-free and Brownian rotational diffusion spaces. *J. Biomol. NMR 40*, 107−119.

(33) d'Auvergne, E., and Gooley, P. (2008) Optimisation of NMR dynamic models II. A new methodology for the dual optimization of the model-free parameters and the Brownian rotational diffusion tensor. *J. Biomol. NMR 40*, 121−133.

(34) Walker, O., Varadan, R., and Fushman, D. (2004) Efficient and accurate determination of the overall rotational diffusion tensor of a molecule from ^{15}N relaxation data using computer program ROTDIF. *J. Magn. Reson. 168*, 336−345.

(35) Long, D., Liu, M., and Yang, D. (2008) Accurately Probing Slow Motions on Millisecond Timescales with a Robust NMR Relaxation Experiment. *J. Am. Chem. Soc. 130*, 2432−2433.

(36) Carver, J. P., and Richards, R. E. (1972) A general two-site solution for the chemical exchange produced dependence of T2 upon the carr-Purcell pulse separation. *J. Magn. Reson. 6*, 89−105.

(37) Price, K. V., Storn, R. M., and Lampinen, J. A. (2005) *Differential Evolution*, Springer-Verlag, Berlin.

(38) Kim, P. S., and Baldwin, R. L. (1982) Influence of charge on the rate of amide proton exchange. *Biochemistry 21*, 1−5.

(39) Neuhaus, D., and Williamson, M. P. (1989) *The nuclear Overhauser effect in structural and conformational analysis*, VCH Publishers Ltd., Chichester, U.K.
(40) Smirnov, S. N., Golubev, N. S., Denisov, G. S., Benedict, H., Schah-Mohammedi, P., and Limbach, H.-H. (1996) Hydrogen/Deuterium Isotope Effects on the NMR Chemical Shifts and Geometries of Intermolecular Low-Barrier Hydrogen-Bonded Complexes. *J. Am. Chem. Soc. 118*, 4094−4101.
(41) Pelton, J. G., Torchia, D. A., Meadow, N. D., and Roseman, S. (1993) Tautomeric states of the active-site histidines of phosphorylated and unphosphorylated IIIGlc, a signal-transducing protein from *Escherichia coli*, using two-dimensional heteronuclear NMR techniques. *Protein Sci. 2*, 543−558.
(42) Markus, M. A., Dayie, K. T., Matsudaira, P., and Wagner, G. (1996) Local mobility within villin 14T probed via heteronuclear relaxation measurements and a reduced spectral density mapping. *Biochemistry 35*, 1722−1732.
(43) Labeikovsky, W., Eisenmesser, E. Z., Bosco, D. A., and Kern, D. (2007) Structure and Dynamics of Pin1 During Catalysis by NMR. *J. Mol. Biol. 367*, 1370−1381.
(44) Bailey, M. L., Shilton, B. H., Brandl, C. J., and Litchfield, D. W. (2008) The Dual Histidine Motif in the Active Site of Pin1 Has a Structural Rather than Catalytic Role. *Biochemistry 47*, 11481−11489.
(45) Zhou, P., Tian, F., Lv, F., and Shang, Z. (2009) Geometric characteristics of hydrogen bonds involving sulfur atoms in proteins. *Proteins 76*, 151−163.
(46) Sultana, R., Boyd-Kimball, D., Poon, H. F., Cai, J., Pierce, W. M., Klein, J. B., Markesbery, W. R., Zhou, X. Z., Lu, K. P., and Butterfield, D. A. (2006) Oxidative modification and down-regulation of Pin1 in Alzheimer's disease hippocampus: A redox proteomics analysis. *Neurobiol. Aging 27*, 918−925.
(47) Dalle-Donne, I., Rossi, R., Giustarini, D., Milzani, A., and Colombo, R. (2003) Protein carbonyl groups as biomarkers of oxidative stress. *Clin. Chim. Acta 329*, 23−38.
(48) Hall, D. A., Vander Kooi, C. W., Stasik, C. N., Stevens, S. Y., Zuiderweg, E. R., and Matthews, R. G. (2001) Mapping the interactions between flavodoxin and its physiological partners flavodoxin reductase and cobalamin-dependent methionine synthase. *Proc. Natl. Acad. Sci. U.S.A. 98*, 9521−9526.